Structural characterization of the PPIase domain of FKBP51, a cochaperone of human Hsp90

Andreas Bracher,[a]* Christian Kozany,[b] Ann-Katrin Thost[a] and Felix Hausch[b]*

[a]Department of Cellular Biochemistry, Max Planck Institute of Biochemistry, Am Klopferspitz 18, 82152 Martinsried, Germany, and [b]Chemical Genomics Research Group, Max Planck Institute of Psychiatry, Kraepelinstrasse 2–10, 80804 Munich, Germany

Correspondence e-mail: bracher@biochem.mpg.de, hausch@mpipsykl.mpg.de

Steroid hormone receptors are key components of mammalian stress and sex hormone systems. Many of them rely on the Hsp90 chaperone system for full function and are further fine-tuned by Hsp90-associated peptidyl–prolyl isomerases such as FK506-binding proteins 51 and 52. FK506-binding protein 51 (FKBP51) has been shown to reduce glucocorticoid receptor signalling and has been genetically associated with human stress resilience and with numerous psychiatric disorders. The peptidyl–prolyl isomerase domain of FKBP51 contains a high-affinity binding site for the natural products FK506 and rapamycin and has further been shown to convey most of the inhibitory activity on the glucocorticoid receptor. FKBP51 has therefore become a prime new target for the treatment of stress-related affective disorders that could be amenable to structure-based drug design. Here, a series of high-resolution structures of the peptidyl–prolyl isomerase domain of FKBP51 as well as a cocrystal structure with the prototypic ligand FK506 are described. These structures provide a detailed picture of the drug-binding domain of FKBP51 and the molecular binding mode of its ligand as a starting point for the rational design of improved inhibitors.

1. Introduction

The hormone-mediated activation of steroid receptors is a crucial process to convey endocrine signals in animals. In the absence of the respective hormone, the ligand-binding domains of many steroid receptors are not stably folded and are turned over rapidly by the protein-folding and degradation machinery in the cytosol. The maturation of the steroid receptors to the hormone-binding competent conformation is mediated by the Hsp70 and Hsp90 molecular-chaperone systems (Echeverria & Picard, 2010). The partially folded receptors are initially recognized and processed by Hsp70 and subsequently handed over to Hsp90 with the help of HOP (Hsp70–Hsp90 organizing protein), which is thought to serve as an adaptor between the molecular chaperones. In the Hsp90-bound state the steroid receptor matures by an unknown mechanism, becoming competent for hormone activation. Upon binding of the hormone, the steroid receptor is transported into the nucleus, where it binds to hormone-responsive elements in the chromosomes, resulting in altered gene expression. Numerous Hsp90 cochaperones have been found to be associated with Hsp90–steroid receptor complexes. Among these factors, peptidyl–prolyl *cis–trans* isomerases (PPIases) appear to be particularly important for

the maturation process of steroid hormone receptors (Pratt *et al.*, 2008; Smith & Toft, 2008). All Hsp90-associated PPIases are multi-domain proteins comprising a TPR-clamp domain which mediates the association with Hsp90 through recognition of its C-terminal EEVD sequence motif, while the remaining parts of the proteins appear to confer specificity to the Hsp90-bound client protein.

The human PPIase FKBP52 enhances the hormone activation of human steroid hormone receptors such as the glucocorticoid receptor (GR). In mice it has been shown to be crucial for fertility and for correct sexual development, likely by enabling optimal signalling of the androgen or progesterone receptor (Cheung-Flynn *et al.*, 2005; Tranguch *et al.*, 2005; Yang *et al.*, 2006; Yong *et al.*, 2007). Interestingly, the closely related FKBP51 has an opposing effect on the glucocorticoid receptor in most cell types. Comparatively high levels of the inhibitory FKBP51 in New World monkeys contribute to the reduced responsiveness to cortisol in these animals (Westberry *et al.*, 2006). In humans, single-nucleotide polymorphisms in the gene encoding FKBP51 are genetically associated with various stress-related psychiatric disorders and with altered expression of FKBP51 (Binder, 2009). Thus, FKBP51 has emerged as a promising novel pharmacological target for the treatment of psychiatric disorders. Recently, FKBP51 has also been shown by two independent groups to enhance androgen receptor signalling in prostate cancer cell lines in an FK506-sensitive manner (Ni *et al.*, 2010; Periyasamy *et al.*, 2010). If these findings can be confirmed in animal models, FKBP51 inhibition could become an exciting new therapeutic option for prostate cancer.

The sequences of the human PPIases FKBP51 and FKBP52 are 55% identical. The two proteins share a common domain structure consisting of an N-terminal FK506-binding PPIase (FKBP) domain, an FKBP-like domain and a C-terminal TPR-clamp domain (Fig. 1*a*). The human genome encodes at least 17 FKBP-domain proteins apparently acting in distinct functional contexts (Galat, 2008). Their common ligand FK506 acts as an immunosuppressive drug by mediating nonphysiological association of the most abundant FKBP protein FKBP12 and possibly also FKBP12.6 and FKBP51 with calcineurin (Weiwad *et al.*, 2006). The latter is required for the activation of NF-AT, which in turn is crucial for the activation of T cells. Similarly, binding of the structurally related drug rapamycin to FKBP12 triggers an inhibitory association with mTOR. Binding of FK506 or rapamycin to FKBP51 or FKBP52 inhibits their PPIase and hormone receptor modulation activities. While the molecular mechanism of steroid hormone receptor modulation and in particular the antagonistic effect of FKBP51 *versus* FKBP52 are not understood, it is clear that the FK506-binding domains play a prominent role. While the PPIase activity *per se* does not appear to be necessary for steroid hormone receptor modulation, a single amino-acid swap at the periphery of the FK506-binding site (L119P) was sufficient to diminish and partially reverse the inhibitory or stimulatory effect of FKBP51 and FKBP52, respectively (Riggs *et al.*, 2007). The FK506-binding pocket thus appears to be a critical part of the interaction area with the Hsp90–GR complex.

The PPIase domain of the prototypic FKBP12 has been the subject of intensive structural investigation because of its role as a mediator of immunosuppression by FK506 and rapamycin (Becker *et al.*, 1993; Van Duyne, Standaert, Karplus *et al.*, 1991; Van Duyne, Standaert, Schreiber *et al.*, 1991; Wilson *et al.*, 1995). FKBP12 has also been the target of several structure-based drug-design programs (Dornan *et al.*, 2003). The structures of full-length FKBP51 from squirrel monkey and human have been solved in the apo form. The two structures exhibit very similar crystal packing, with the three domains forming a linear array in each structure (Sinars *et al.*, 2003). A very similar domain orientation has also been observed in the crystal structures of a construct comprising the FKBP and FKBP-like domains of FKBP52, suggesting that the array observed for FKBP51 represents the preferred domain arrangement for both FKBP51 and FKBP52 (Wu *et al.*, 2004). Unfortunately, the FK506-binding domain of full-length FKBP51 is poorly ordered in the published crystal structures. Specifically, 43 and 51 (of 138) residues are missing in the models, respectively, preventing a detailed structural comparison with FKBP52 and other FKBP domains. Furthermore, the FK506-binding pocket is blocked by a crystal contact in this crystal form, excluding analysis of the interactions with bound inhibitors. Such complexes would however be of great importance for the rational design of chemical compounds targeting FKBP51. We thus set out to find a better suited crystal form of FKBP51.
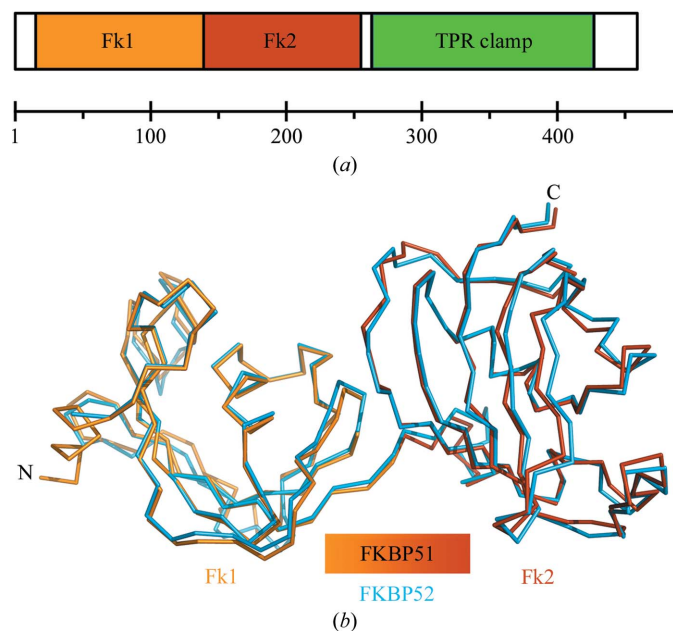

Figure 1
Domain structure of FKBP51. (*a*) Domain composition of FKBP51. The ruler indicates the residue numbers. (*b*) Superposition of the FKBP51(1–260) fragment crystal structure with the corresponding FKBP52 crystal structure (PDB entry 1q1c; Wu *et al.*, 2004). The backbone traces of the FK1 and FK2 domains of one FKBP51 chain are shown in orange and red, respectively. The two copies of FKBP51(1–260) in the asymmetric unit are almost identical. The backbone of FKBP52(1–260) is indicated in blue. The positions of the chain termini are indicated.

2. Materials and methods

2.1. Expression constructs

Plasmids harbouring the cDNA of human FKBP51 were kindly provided by Dr Theo Rein (Max Planck Institute for Psychiatry, Munich, Germany). The DNA sequence corresponding to amino acids 1–140 of FKBP51 was PCR-amplified with the primers 5′-CAT GCC ATG GCA ATG ACT ACT GAT G-3′ and 5′-GCA GTC GAC TCA CTC TCC TTT GAA ATC AAG GAG C-3′. For the cloning of amino acids 1–260 of FKBP51, the following reverse primer was used: 5′-GCA GTC GAC TCA ATC CAT CTC CCA GGA TTC TTT G-3′. Both constructs were cloned into the pProEx-Hta plasmid (Invitrogen, Carlsbad, USA) using the restriction enzymes NcoI and SalI. For cloning FKBP51 constructs starting at position 16 using the EheI restriction site, the forward primers 5′-GCC CCG GCC ACT GTT GCT GAG CAG GGA G-3′ (introducing the A19T mutation) and 5′-GCC CCG GCC GCT GTT ACT GAG CAG GGA G-3′ were employed.

2.2. Protein expression and purification

Escherichia coli BL21 (DE3) strain pLysS was used as the expression host for FKBP51 constructs starting at residue 1. Protein expression was induced at 310 K for 3 h by addition of 0.6 mM IPTG. The proteins were purified by Ni–NTA chromatography (Qiagen, Hilden, Germany) essentially according to the manufacturer's protocol but with some modifications. The wash and elution buffers consisted of 25 mM NaCl, 10% glycerol and 30 or 300 mM imidazole, respectively. The His$_6$ tag was cleaved using His$_6$-TEV protease [1/100(w/w)]. After the removal of imidazole by gel filtration using PD10 columns (GE Healthcare, Waukesha, USA), the protease and uncleaved proteins were separated by a second Ni–NTA chromatography step.
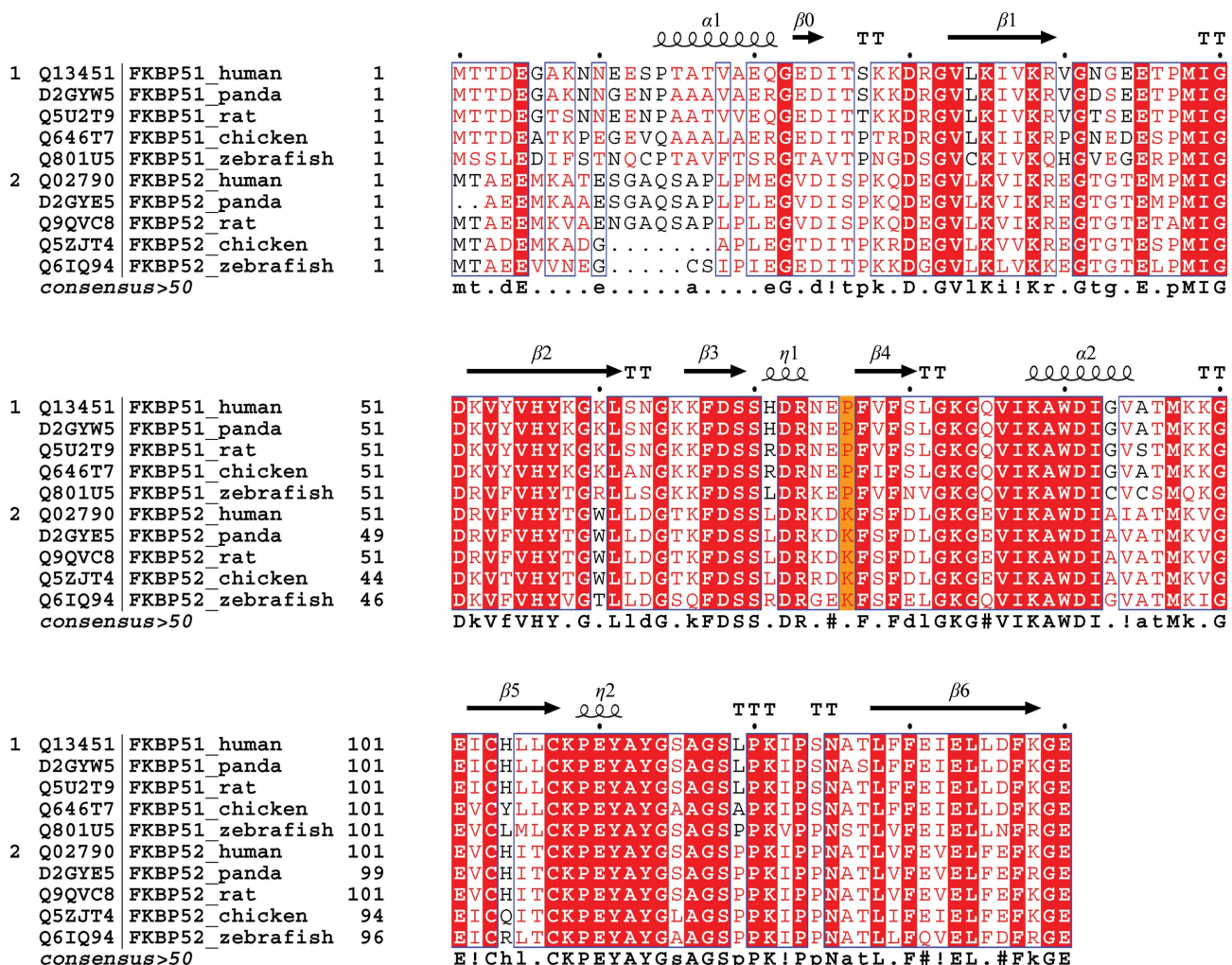

Figure 2
Sequence alignment of the FK506-binding domains of FKBP51 and FKBP52. Amino-acid sequences of selected FKBP51 and FKBP52 homologues (groups 1 and 2, respectively) were aligned using *ClustalX*. Secondary-structure elements and numbering for FKBP51 are indicated above the sequences. Similar residues are shown in red and identical residues are shown in bold lettering on a red background. Blue frames indicate homologous regions. The orange background highlights systematic differences between FKBP51 and FKBP52 sequences. The consensus sequence is shown at the bottom. UniProt accession numbers are indicated.

Table 1
Data-collection and refinement statistics.

Parameters are as defined in *SCALA*. Values in parentheses are for the outer shell.

PDB code	3o5d	3o5e	3o5f	3o5g	3o5i	3o5j	3o5k
FKBP51 construct	1–260	1–140	1–140	16–140	16–140	16–140	16–140
Crystal packing type	V	VI	VII	I	II	III	VIII
Ligand	—	—	—	—	—	—	—
Crystallization buffer	0.2 M (NH$_4$)$_3$ citrate pH 7.0, 20% PEG 3350	1.8 M (NH$_4$)$_3$ citrate pH 7.0	30% PEG 2000 MME, 0.1 M KSCN	35% PEG 3350, 0.1 M HEPES–NaOH pH 7.5	35% PEG 3350, 0.2 M NH$_4$ acetate, 0.1 M HEPES–NaOH pH 7.5	29% PEG 3350, 0.1 M HEPES–NaOH pH 7.5	32% PEG 3350, 0.05 M NH$_4$ acetate, 0.1 M HEPES–NaOH pH 7.5
Synchrotron	ESRF	SLS	SLS	ESRF	ESRF	ESRF	ESRF
Beamline	ID29	X10SA	X10SA	ID14-4	ID14-4	ID23-1	ID14-4
Space group	$I4_1$	$P3_2 21$	$P2_1 2_1 2_1$	$P3_2 21$	$P3_1 21$	$P2_1 2_1 2_1$	$P2_1$
Unit-cell parameters							
a (Å)	113.73	54.38	35.68	46.99	48.35	35.29	69.80
b (Å)	113.73	54.38	49.70	46.99	48.35	48.80	48.43
c (Å)	112.13	90.15	66.98	89.77	180.48	64.30	76.32
α (°)	90	90	90	90	90	90	90
β (°)	90	90	90	90	90	90	114.49
γ (°)	90	120	90	120	120	90	90
Integration software	*IPMOSFLM/ SCALA*	*IPMOSFLM/ SCALA*	*IPMOSFLM/ SCALA*	*IPMOSFLM/ SCALA*	*IPMOSFLM/ SCALA*	*IPMOSFLM/ SCALA*	*IPMOSFLM/ SCALA*
Resolution limits (Å)	35.97–4.0 (4.22–4.0)	41.74–1.6 (1.69–1.6)	39.90–1.65 (1.74–1.65)	89.80–2.0 (2.11–2.0)	41.89–1.8 (1.9–1.8)	64.28–1.7 (1.79–1.7)	69.51–2.7 (2.85–2.7)
R_{merge}	0.177 (0.710)	0.086 (0.409)	0.049 (0.455)	0.091 (0.667)	0.094 (0.417)	0.064 (0.361)	0.088 (0.392)
$\langle I/\sigma(I)\rangle$	6.4 (2.2)	10.8 (3.0)	14.2 (2.7)	17.4 (2.7)	13.9 (3.7)	21.4 (4.1)	11.6 (3.4)
Multiplicity	3.4 (3.4)	4.4 (4.4)	3.5 (3.4)	6.6 (6.9)	5.1 (5.2)	6.6	3.5 (3.6)
Completeness (%)	99.6 (99.8)	99.9 (100)	99.3 (98.6)	99.9 (100)	99.7 (99.8)	99.8 (100)	99.3 (99.7)
Wilson B factor (Å^2)	n.a.	20.19	23.31	30.44	19.22	22.44	53.37
Refinement program	*REFMAC*	*REFMAC*	*REFMAC*	*REFMAC*	*REFMAC*	*REFMAC*	*REFMAC*
Resolution range (Å)	20–4.0	20–1.6	20–1.65	20–2.0	20–1.8	20–1.7	20–2.7
Reflections	5748	19850	14004	7809	22317	12132	12261
Reflections in test set	275	1076	748	376	1213	624	629
R_{cryst}	0.317	0.189	0.197	0.191	0.203	0.201	0.224
R_{free}	0.344	0.229	0.238	0.266	0.246	0.231	0.283
No. of atoms	3742	1165	1118	1039	2118	996	3794
R.m.s.d. bonds (Å)	0.006	0.012	0.013	0.011	0.013	0.012	0.010
R.m.s.d. angles (°)	0.815	1.441	1.413	1.384	1.382	1.384	1.223
Ramachandran plot† (%)							
Most favoured	87.4	96.2	94.3	94.3	93.4	90.4	87.3
Additional allowed	12.6	2.8	3.8	3.8	5.2	8.7	11.6

FKBP51 constructs starting at residue 16 were expressed in *E. coli* BL21 (DE3) Codon Plus RIL. The proteins were purified by tandem Ni-affinity chromatography on Chelating Sepharose (GE Healthcare) using buffer consisting of 20 mM HEPES–KOH pH 7.4, 200 mM KCl and 4 mM MgCl$_2$ and were separated by a TEV protease cleavage step. Subsequently, the purified proteins were applied onto a Superdex 200 size-exclusion chromatography column which was equilibrated with buffer consisting of 20 mM Tris–HCl pH 8.0 and 50 mM NaCl. FKBP51-containing fractions were pooled and concentrated to 10–30 mg ml^{-1} by ultrafiltration.

2.3. Crystallization

Index screen (Hampton Research, Aliso Viejo, California, USA) was employed to identify crystallization conditions at 293 K using the hanging-drop vapour-diffusion method. The FKBP51(16–140)-A19T–FK506 complex was formed by mixing 100 µl FKBP51(16–140)-A19T at 30 mg ml^{-1} with 4 µl DMSO containing 50 mM FK506. The exact crystallization conditions are listed in Table 1.

2.4. Structure solution and refinement

Diffraction data were collected at the European Synchrotron Radiation Facility (ESRF), Grenoble, France and the Swiss Synchrotron Light Source (SLS), Villigen, Switzerland (see Table 1 for details). Diffraction data were integrated with *MOSFLM* (Leslie, 1992) or *XDS* (Kabsch, 2010) and further processed with *SCALA* (Evans, 1997) and *TRUNCATE* (French & Wilson, 1978) as implemented in the *CCP*4*i* interface (Winn *et al.*, 2011; Potterton *et al.*, 2003). The crystal structures were solved by molecular replacement employing the program *MOLREP* (Vagin & Teplyakov, 2010). Model bias was reduced by automated model building with *ARP/ wARP* v.6.1 (Perrakis *et al.*, 1999). Subsequent iterative model improvement and refinement were performed with *Coot* and *REFMAC*5 (Murshudov *et al.*, 2011) or *SHELXL* (Sheldrick, 2008), respectively. The dictionary for FK506 was generated with the *PRODRG* server (Schüttelkopf & van Aalten, 2004). Residues facing solvent channels without detectable side-chain density were modelled as alanines.

Coordinates were aligned with *LSQMAN* and *THESEUS* (Theobald & Wuttke, 2006*a,b*, 2008). The sequence-alignment

Table 1 (continued)

PDB code	3o5l	3o5m	3o5o	3o5p	3o5q	3o5r
FKBP51 construct	16–140 A19T	16–140 A19T	16–140 A19T	16–140 A19T	16–140 A19T	16–140 A19T
Crystal packing type	I	II	III	IV	IV	IV
Ligand	–	–	–	–	–	FK506
Crystallization buffer	30% Jeffamine ED-2001, 0.1 M HEPES–NaOH pH 7.0	32% PEG 3350, 0.05 M NH$_4$ acetate, 0.1 M bis-tris–HCl pH 6.5	33% PEG 3350, 0.05 M KSCN, 0.1 M bis-tris–HCl pH 6.5	25% PEG 3350, 0.2 M NH$_4$ acetate, 0.1 M HEPES–NaOH pH 7.5	38% PEG 3350, 0.1 M NH$_4$ acetate, 0.1 M HEPES–NaOH pH 7.5, 10% DMSO	25% PEG 3350, 0.2 M NH$_4$ acetate, 0.1 M HEPES–NaOH pH 7.5
Synchrotron	SLS	SLS	SLS	SLS	ESRF	ESRF
Beamline	X10SA	X10SA	X10SA	X10SA	ID14-4	ID23-1
Space group	$P3_221$	$P3_121$	$P2_12_12_1$	$P2_12_12_1$	$P2_12_12_1$	$P2_12_12_1$
Unit-cell parameters						
a (Å)	47.98	48.77	35.70	42.29	42.40	42.05
b (Å)	47.98	48.77	48.24	54.30	53.63	54.78
c (Å)	89.00	179.99	62.95	56.65	56.54	56.82
α (°)	90	90	90	90	90	90
β (°)	90	90	90	90	90	90
γ (°)	120	120	90	90	90	90
Integration software	IPMOSFLM/SCALA	IPMOSFLM/SCALA	IPMOSFLM/SCALA	IPMOSFLM/SCALA	XDS/SCALA	IPMOSFLM/SCALA
Resolution limits (Å)	30.37–1.3 (1.37–1.3)	45.00–1.6 (1.69–1.6)	38.29–1.15 (1.21–1.15)	25.11–1.0 (1.06–1.0)	33.92–0.96 (1.01–0.96)	28.77–1.1 (1.16–1.1)
R_{merge}	0.063 (0.399)	0.076 (0.395)	0.047 (0.325)	0.044 (0.164)	0.032 (0.300)	0.079 (0.471)
$\langle I/\sigma(I)\rangle$	13.1 (2.7)	13.2 (2.9)	17.7 (3.2)	21.0 (6.4)	19.7 (3.5)	14.7 (3.7)
Multiplicity	4.1 (3.8)	4.7 (4.6)	4.9 (3.2)	4.2 (3.0)	3.5 (2.9)	6.7 (6.6)
Completeness (%)	99.1 (98.2)	96.7 (96.1)	98.3 (95.1)	87.8 (57.6)	94.6 (88.3)	99.8 (99.8)
Wilson B factor (Å^2)	14.32	17.18	7.57	7.08	5.19	6.38
Refinement program	REFMAC	REFMAC	SHELXL	SHELXL	REFMAC	SHELXL
Resolution range (Å)	20–1.3	20–1.6	20–1.15	20–1.0	20–0.96	20–1.1
Reflections	28029	31010	36627	58981	70534	51159
Reflections in test set	1487	1660	1922	3122	3687	2694
R_{cryst}	0.172	0.200	0.123	0.116	0.130	0.123
R_{free}	0.206	0.236	0.161	0.147	0.153	0.157
No. of atoms	1241	2179	1255	1449	1381	1470
R.m.s.d. bonds (Å)	0.015	0.013	0.014	0.014	0.014	0.019
R.m.s.d. angles (°)	1.554	1.468	2.151	2.179	1.546	2.398
Ramachandran plot† (%)						
Most favoured	90.6	92.9	96.2	91.5	93.4	95.3
Additional allowed	8.5	6.1	2.8	7.5	5.7	3.8

† As defined in PROCHECK (Laskowski et al., 1993).

figure (Fig. 2) was prepared with *ESPript* (Gouet *et al.*, 1999). Molecular-graphics figures were generated with the program *PyMOL* (DeLano, 2002).

Coordinates and structure-factor amplitudes were deposited in the Protein Data Bank; see Table 1 for accession codes.

3. Results and discussion

3.1. Design of a FKBP51 crystallization construct suitable for cocrystallization studies

Since FKBP52 is highly homologous to FKBP51, we thought that similar strategies in construct design might yield better suited crystals of FKBP51. Crystals of constructs of FKBP52 comprising the FKBP domain (residues 1–140) and both the FKBP and FKBP-like domains together (residues 1–260) have been reported (Li *et al.*, 2003; Wu *et al.*, 2004). While both had sufficient resolution for inhibitor studies, the FK506-binding pocket of the former was blocked by a crystal contact.

FKBP51(1–260) was efficiently expressed as a soluble fusion protein with a TEV protease-cleavable His$_6$ tag in *E. coli*. After removal of the His$_6$ tag, this construct readily formed large crystals. However, these crystals only diffracted to approximately 4.0 Å resolution. We were able to solve the crystal structure by molecular replacement using the structure of FKBP52(1–260) as a search model, indicating that the FKBP–FKBP-like domain orientation in FKBP51 is indeed very similar to that of FKBP52 (Table 1, Fig. 1b).

Similar to FKBP51(1–260), the FKBP-domain construct FKBP51(1–140) only yielded crystals after proteolytic removal of the His$_6$ affinity tag. Two crystal forms were obtained, one in a trigonal setting and the other in an orthorhombic setting (Table 1); both diffracted to approximately 1.6 Å resolution on SLS beamline PX-II. In the trigonal crystal form the binding pocket is blocked by a crystal contact to a symmetry-equivalent molecule related by a twofold axis. The orthorhombic crystals were perfectly suitable for structural analysis of the binding pocket. However, the crystals from both conditions took months to appear and we therefore set out to further improve the crystallization conditions.

In the structure of FKBP52(1–140) residues 1–15 were found to be disordered. This also coincides with the region that is most poorly conserved between FKBP51 and FKBP52 (Fig. 2). Limited proteolysis of FKBP51(1–140) using subtilisin resulted in an approximate 2.5 kDa shift in apparent mole-

cular weight as judged from SDS–PAGE (data not shown), which is consistent with an N-terminal truncation removing an accessible segment of about 15–20 amino acids. Suspecting that this potentially disordered segment could obscure favorable crystal contacts, we therefore designed a construct comprising residues 16–140.

The FKBP51(16–140) construct crystallized readily and four distinct crystal forms were obtained (Table 1). Two of them exhibited unit-cell parameters that were very similar to those of the FKBP51(1–140) crystal forms. The most frequently observed crystal form had a trigonal unit cell in which the c-axis length was doubled compared with the other trigonal lattice because of a pseudo-translation in this direction. The binding pockets were accessible in all crystal forms of FKBP51(16–140). The resolution limits of three of the crystal forms were similar, 2.0–1.7 Å, and thus sufficient for ligand-binding studies. The fourth crystal form was monoclinic, comprising four molecules per asymmetric unit.

During initial PCR cloning of the FKBP51(16–140) expression construct a clone with the mutation A19T was obtained. Serendipitously, this mutated construct FKBP51(16–140)-A19T happened to yield crystals of far superior quality. Four crystal forms were obtained, diffracting to between 1.6 and 0.96 Å resolution (Table 1). Three of these were isomorphous to FKBP51(16–140) crystal-packing types I–III. Crystal

Figure 3
The point mutation A19T enables a favourable crystal contact. This close-up shows the favourable crystal contact in type IV orthorhombic crystals of the FKBP51(16–140) A19T mutant (PDB entry 3o5q). Protein backbones are shown in ribbon representation and side chains are shown in stick representation. Blue and white colours denote the two molecules. N and O atoms are indicated in bright blue and red, respectively. The blue molecule is enveloped by the van der Waals surface to highlight the surface shape complementarity. The hydrogen bond between residues Thr19 and Asn74 is indicated by a dashed line. Residues close to the crystal contact are labelled. Residues Ser62 and Arg73 exhibit alternative side-chain conformations in the crystal structure.

form IV, which had a distinct orthorhombic lattice, was the most reproducible, regularly yielding large single crystals that diffracted to approximately 1.0 Å resolution. Residue 19 is located at the interface between an α-helix at the N-terminus and the body of the FKBP domain. The side chain of the preceding residue Val18 points into a hydrophobic pocket formed by residues Leu34, Ile36, His104, Leu106 and Phe129. The A19T mutation creates additional van der Waals contacts to Leu106, which might rigidify the N-terminal section of FKBP51 to some extent. In the best crystal form, form IV, the γ-hydroxyl group of Thr19 forms a short hydrogen bond to the side chain of Asn74 from a symmetry-related protein molecule, enabling a tight crystal contact (Fig. 3). Leu106 had a different side-chain conformation in this crystal form, packing tightly against Thr127. Thus, for crystal form IV these additional interactions might result in better packing and consequently higher diffraction power. Table 1 gives an overview of the observed crystal forms.

3.2. Structure of the FKBP51 FK506-binding domain

The FK506-binding domain of FKBP51 comprises residues 15–138. Similar to other FKBP-domain structures (Dornan et al., 2003; Galat, 2008), the structure of the FK506-binding domain of FKBP51 consists of a curved five-stranded antiparallel β-sheet wrapping around a central α-helix, α2, which is inserted after the third β-segment (this strand is interrupted by a bulge in FKBP51 and is thus assigned as β3 and β4 in secondary-structure element numbering; Fig. 4a). In addition, a short α-helix is found at the N-terminus of the FK506-binding domain of FKBP51, which is situated across β-strands β1, β5 and β6. The interface between this helix and the β-sheet is extended and hydrophobic, indicating that this helix is an integral component of the domain and helix formation is not only forced by crystal contacts. Consistent with this notion, helix α1 was observed in every crystal form studied apart from the previously reported full-length FKBP51 crystal structures; however, in these structures the whole FK1 domains were poorly defined (Sinars et al., 2003). Reassessment of the structure of full-length human FKBP51 showed that a model comprising the complete FK1 domain had considerably better refinement statistics than the fragmentary model (R_{free} of 0.322 versus R_{free} of 0.339 using the same refinement protocol), indicating that helix α1 is indeed an integral part of the N-terminal domain (data not shown). The residues 1–12 upstream of helix α1 were disordered in the structures of FKBP51(1–140), consistent with the poor sequence conservation in this segment. The linker following helix α1 forms a short antiparallel extension to the five-stranded β-sheet separated by an extended loop (residues 25–32). Systematic analysis of the conformational variation of the FK506-binding domains in the different crystal forms using THESEUS suggests that the conformation of this peripheral loop is very well defined (Fig. 4b), similar to the β-sheet and the central helix α2. Regions of increased structural plasticity are found in the peripheral parts of the domain structure: these are the chain termini, the region comprising residues 42–45, the β-turn
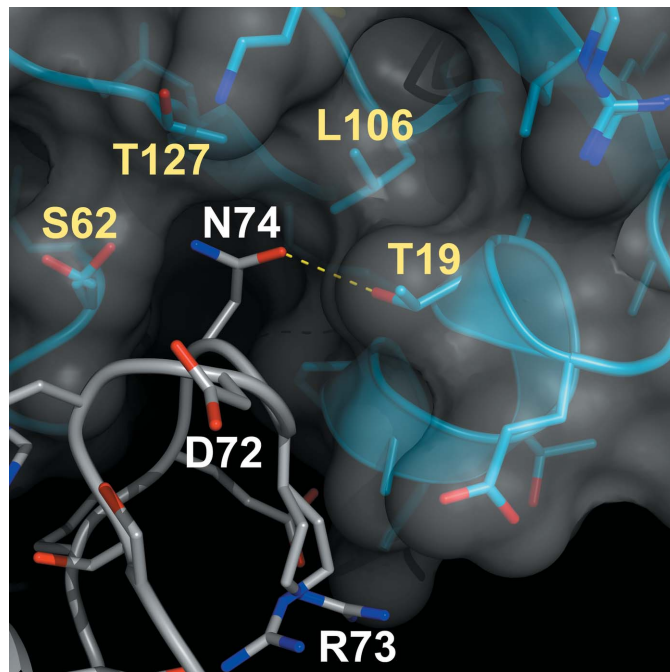
between β2 and β3 (residues 61–65), the bulge between β3 and β4 (71–74) and the tip of the extended loop connection between β5 and β6 (118–122). The latter loop and the bulge flank a deep hydrophobic pocket (the presumed PPIase active site) located at the N-terminus of helix α2 and might thus modulate substrate sequence specificity (Fig. 4c).

All FKBP51 FK1-domain structures contain one clear Ramachandran plot outlier: residue Ala112. This conformation is fully warranted by the electron density and is not a refinement artifact. The unusual conformation is apparently forced by the packing constraints for the bulky side chains of the flanking tyrosine residues Tyr111 and Tyr113 in the hydrophobic interior of the domain. This segment is a hallmark of the FKBP family (Galat, 2008) and its conformation is completely conserved between FKBP51 and FKBP52 as well as several other FKBPs, underscoring its functional importance (Fig. 2).

3.3. Comparison with the FK506-binding domain of FKBP52

The most prominent difference between the FKBP domains of FKBP51 and FKBP52 is the presence of the N-terminal α1 helix in FKBP51, while the corresponding region of FKBP52 was disordered in the crystal structures (Fig. 4d). In the respective sequence segment, FKBP52 contains two proline residues, Pro17 and Pro19, which are not compatible with an α-helical structure (Fig. 2). Interestingly, the hydrophobic patch on the β-sheet that forms the interface to helix α1 is largely preserved in FKBP52 and thus might serve as a secondary binding site for partially folded substrate proteins. Alternatively, this region could provide a docking site for FKBP52-specific protein interaction partners such as dynamitin, which is believed to facilitate dynamin-dependent retrograde transport of steroid receptors after hormone binding (Galigniana et al., 2004). Whether the N-terminal helix of FKBP51 can allosterically influence the dynamics of the adjacent loops (e.g. Ser62–Lys65) remains to be determined. Apart from the N-terminal segment, the structures differ only locally. The most conspicuous differences were found close to the bulge between β3 and β4 (71–74) and in the extended loop connection between β5 and β6 (118–122). In the former, residue Pro76 in FKBP51 (instead of Lys76 in FKBP52) enforces a distinct conformation. In the 118–122 loop, all
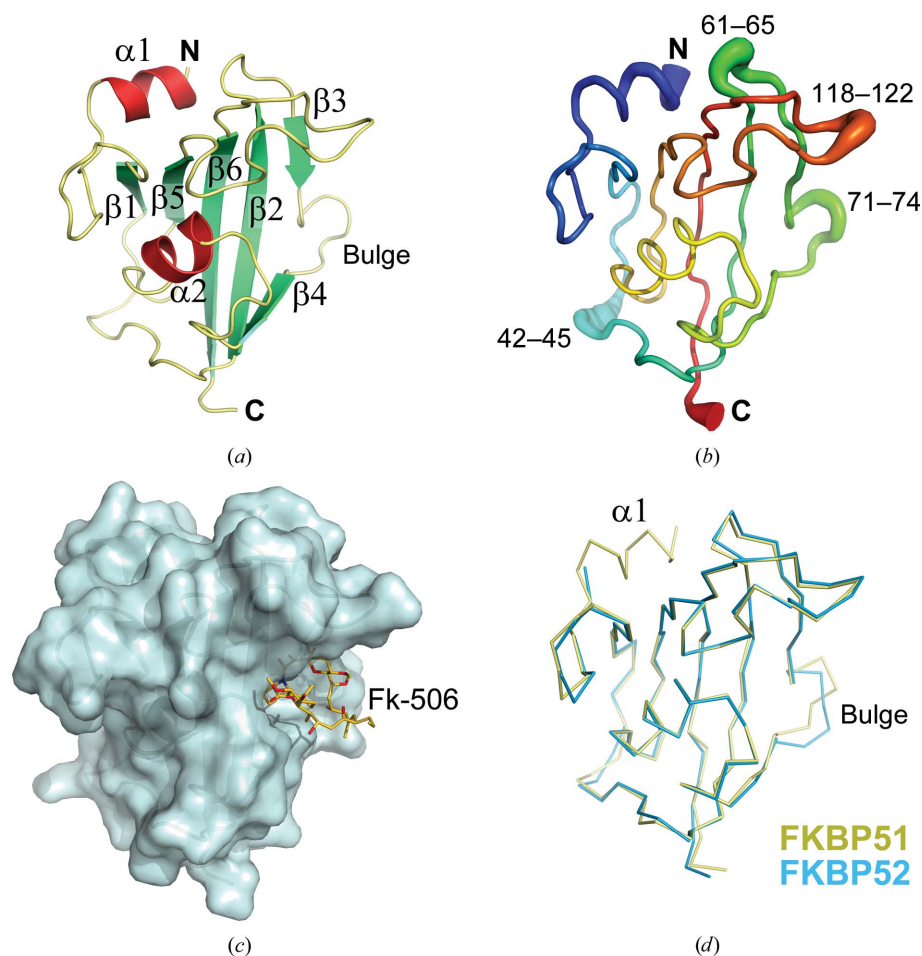

Figure 4
Crystal structure of the FK506-binding domain of FKBP51. (a) Ribbon representation of the median FKBP51 FK1-domain structure (PDB entry 3o5i). α-Helices and β-strands are indicated in red and green, respectively. Chain termini and secondary-structure elements are labelled. (b) Structural plasticity of the FKBP51 FK1-domain structure. The program THESEUS was used to superpose the different FKBP51 data sets and map the local structural divergence onto the backbone (Theobald & Wuttke, 2006a,b, 2008). Thickening indicates increased conformational divergence. The most diverse regions are labelled by residue number. The orientation is the same as in (a). (c) Surface representation of the FKBP51 FK1-domain structure. A van der Waals envelope of FKBP51 is shown. The location of the substrate-binding pocket is indicated by the superposed inhibitor FK506. (d) Superposition with the FKBP52 FK1-domain structure (PDB entry 1q1c; Wu et al., 2004). The backbone traces of the FK1 domains of FKBP51 and FKBP52 are shown in pale yellow and blue, respectively.

FKBP51 crystal structures contain a cis-peptide bond between Leu119 and Pro120, while both cis and trans configurations appear to be possible for the Pro119–Pro120 peptide bond in FKBP52 (note that FKBP52 sequences contain two conserved diproline motifs in this region). Importantly, the residue at position 119 was found to account for the differing effects of FKBP51 and FKBP52 on steroid hormone receptors to a large extent (Riggs et al., 2007). Whether hydrophobic contacts at this position, the conformational constraints imposed by the additional proline or both mediate these differences remains to be elucidated.

3.4. Comparison with other FK506-binding domains

Comparison of the average structure of the FK506-binding domain of FKBP51 with other known human FKBP-domain

structures (FKBP12, FKBP12.6, FKBP13, FKBP25, FKBP36 and FKBP38) suggests that the peripheral regions around the proline-binding pocket might indeed confer substrate specificity to the homologues. The core structure consisting of the central α-helix and the surrounding five-stranded β-sheet, which forms the structural scaffold for the proline-binding pocket, is very well preserved in all of the structures. The largest differences are observed in the peripheral parts, which are often structurally flexible (Wilson *et al.*, 1995), similar to the findings observed for FKBP51 in this report. FKBP38 does not contain a β-bulge [PDB entries 2awg (J. R. Walker, T. Davis, E. M. Newman, P. Finerty, F. Mackenzie, J. Weigelt, M. Sundstrom, C. Arrowsmith, A. Edwards, A. Bochkarev & S. Dhe-Paganon, unpublished work), 2f2d (Maestre-Martínez *et al.*, 2006) and 3ey6 (Maestre-Martínez *et al.*, 2011)], whereas FKBP25 has a conspicuously extended bulge structure (PDB entry 1pbk; Liang *et al.*, 1996). The relevance of the β-bulge of FKBPs to interaction with protein clients remains to be established. The structures of the larger FKBP homologues FKBP36 (PDB entry 3b7x; J. R. Walker, T. Davis, C. Butler-Cole, R. Paramanathan, J. Weigelt, C. H. Arrowsmith, A. M. Edwards, A. Bochkarev & S. Dhe-Paganon, unpublished work), FKBP38, FKBP51 and FKBP52 all share the anti-parallel extension to the β-sheet close to the N-terminus. Interestingly, the smallest homologue FKBP12 lacks the complete N-terminal extension; its N-terminus corresponds to FKBP51 residue 32 (Van Duyne, Standaert, Schreiber *et al.*, 1991). This part therefore does not appear to be required for structural integrity. FKBP36 has a small α-helix at the N-terminus similar to FKBP51. However, this α-helix packs onto the β-sheet in a distinct manner. N-terminal helices or helix bundles are also found in the structures of bacterial and protozoan homologues (Horstmann *et al.*, 2006; Pereira *et al.*, 2002; Riboldi-Tunnicliffe *et al.*, 2001; Saul *et al.*, 2004). In these structures these helices are needed for dimerization.

3.5. Structure of the complex with FK506

In order to test whether FKBP51 crystal form IV would indeed be suitable for ligand-binding studies, we cocrystallized FKBP51(16–140)-A19T in complex with FK506 under the same conditions (soaking was not attempted because of the poor solubility of FK506 in aqueous buffers; Fig. 5a). Diffraction data from large crystals of this complex were collected to 1.1 Å resolution on ESRF beamline ID29. The resulting difference electron-density map clearly revealed the inhibitor bound to the hydrophobic pocket of FKBP51 (Fig. 5b). At this high resolution single atoms can be discerned such that, for example, the conformation of aliphatic rings can be unambiguously assigned.

FK506 is bound to a deep hydrophobic pocket at the N-terminal end of the central α-helix. Its pipecolate ring, which possibly mimics a proline residue in a substrate peptide, sits at the bottom of the hydrophobic pocket, facing the indole ring of Trp90 (Fig. 5c). The pipecolate carbonyl group is in tight hydrogen-bond contact to the backbone amide of Ile87. Two additional hydrogen bonds were found between the C_8

carbonyl group and the hydroxyl group of Tyr113 and between the tertiary hydroxyl group at C_{10} and the side chain of Asp68. In addition, the O atom of Tyr113 approaches the carbonyl C_1 atom of the pipecolate of FK506 at an angle of 102° with respect to the carbonyl plane. The distance of 3.17 Å is slightly less than the van der Waals distance. The C—O geometry is therefore optimal for an attractive orthogonal dipolar interaction (Paulini *et al.*, 2005). This might be important in forming a positive cooperative network comprising the amide of Ile87, the C_1=O of the FK506 ester, the OH of Tyr113 and the C_8=O of the FK506 amide. Similar contacts were also observed in the cocrystal structures of FKBP12–FK506 (PDB entries 1fkf, 1fkj and 2fke; Becker *et al.*, 1993; Van Duyne, Standaert, Karplus *et al.*, 1991; Wilson *et al.*, 1995), FKBP12–rapamycin (PDB entries 1fkb and 1fkl; Van Duyne, Standaert, Schreiber *et al.*, 1991; Wilson *et al.*, 1995) and FKBP12.6–rapamycin (PDB entry 1c9h; Deivanayagam *et al.*, 2000) as well as in numerous cocrystal structures of FKBP12 and synthetic pipecolate-derived ligands (PDB entries 1fkg, 1fkh, 1fki, 1j4h, 1j4i and 1j4r; Dubowchik *et al.*, 2001; Holt *et al.*, 1993; Sun *et al.*, 2003). This hydrogen-bond/dipolar interaction network therefore seems to be a key feature of ligands of the FKBP family.

We did not observe a direct hydrogen bond between Gln85 and the C_{24} hydroxyl group of FK506, as has been repeatedly observed in FK506–FKBP12 cocrystal structures (PDB entries 1fkf, 1fkj, 2fke, 1yat and 1bkf; Becker *et al.*, 1993; Itoh *et al.*, 1995; Rotonda *et al.*, 1993; Van Duyne, Standaert, Karplus *et al.*, 1991; Wilson *et al.*, 1995). This interaction is instead mediated indirectly by a water molecule in the FKBP51–
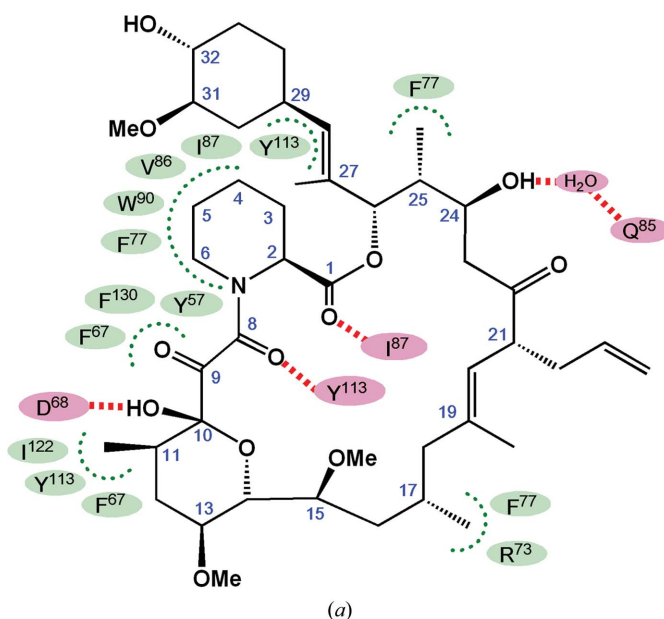

Figure 5
Crystal structure of the complex with FK506. (a) Structural formula of FK506 showing the hydrogen bonds formed to the FK1 domain of FKBP51 in red. Hydrophobic interactions are indicated in green. The atom numbering for FK506 is shown in blue.
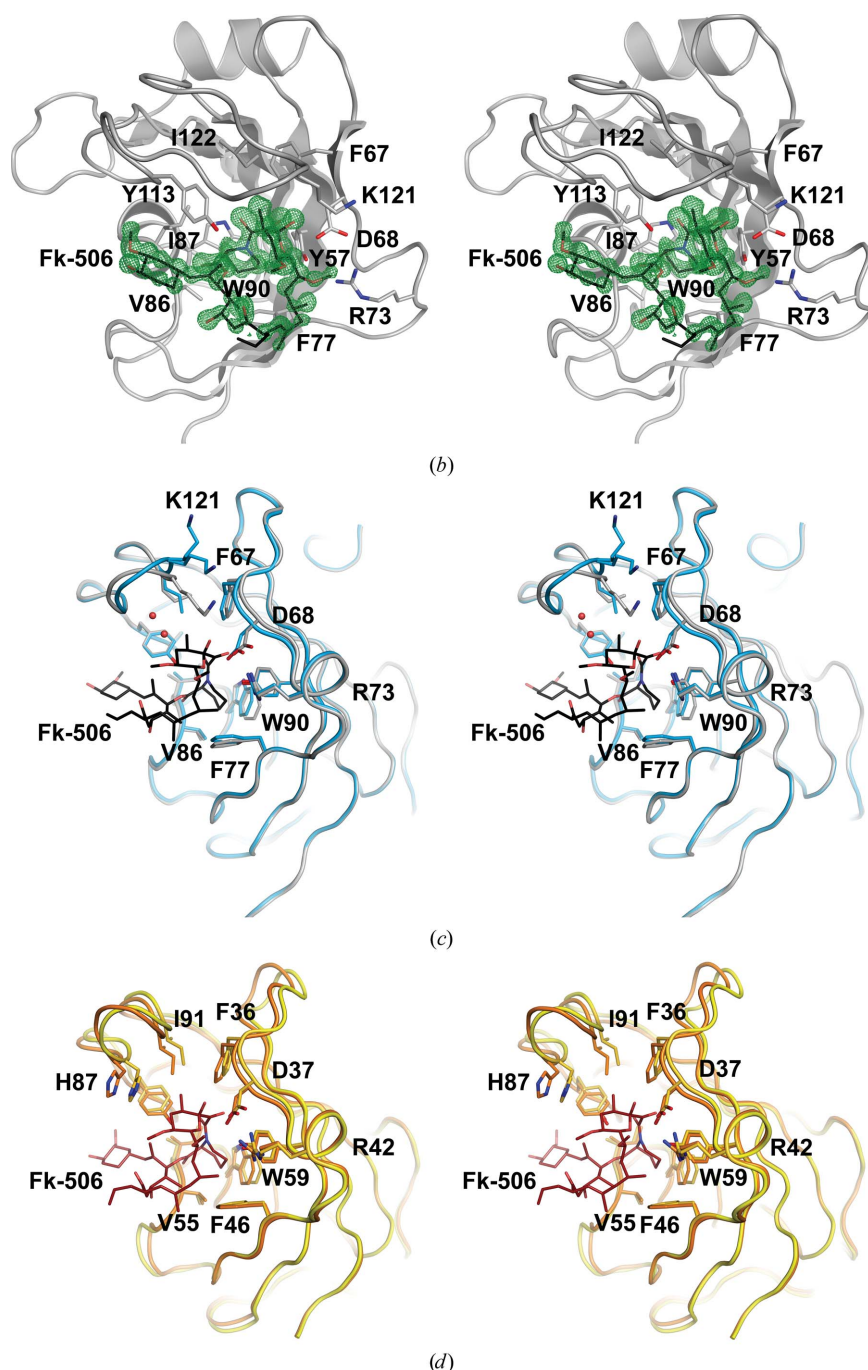
(b)

(c)

(d)

Figure 5 (continued)
(b) Stereo representation of the difference electron density for bound FK506. The $F_o - F_c$ difference density of the FK506 macrocycle at a contour level of 3.0σ is shown as green meshwork. The final FK506 coordinates are shown as a stick model. C, N and O atoms are shown in black, blue and red, respectively. Residues lining the binding pocket are shown in stick representation; the backbone of FKBP51 is shown as ribbons. Binding-pocket residues are labelled. (c) Superposition of the FK506 complex with the apo crystal structure of FKBP51. The FKBP51 structures of FK506-bound and unliganded FKBP51 are shown in grey and blue, respectively. The models are rotated ~45° clockwise around the vertical axis compared with (b). The residues lining the binding pocket are shown in stick representation. The side chain of residue Lys121 assumes two alternative conformations in the apo crystal structure. (d) Superposition of the apo and FK506-bound conformations of FKBP12. For comparison, the corresponding FKBP12 structures were superposed onto FKBP51 using *LSQMAN* and are shown in the same orientation and representation as FKBP51 in (c). The apo and FK506 complex structures are shown in orange and yellow, respectively. FK506 is shown in stick representation; C atoms are indicated in brown.

FK506 complex and is caused by slight movement of the C_{18}–C_{23} tip of FK506. Interestingly, a very similar orientation of the FK506 tip (including a water-mediated C_{24}—OH hydrogen bond) has been observed in the ternary complex FKBP12–FK506–calcineurin (PDB entry 1tco; Griffith *et al.*, 1995). The FK506 in FKBP51 therefore seems to be optimally positioned to engage in a ternary complex with calcineurin and this could contribute to the higher inhibitory activity of the FKBP51–FK506 complex towards calcineurin compared with most other larger FKBP homologues (Weiwad *et al.*, 2006). Similar to FKBP12, the C_9 keto group of FK506 interacts with an unusual pocket formed by edges of the conserved aromatic residues Tyr57, Phe67 and Phe130.

Mostly van der Waals contacts were observed at the rim of the binding pocket. The 32-hydroxy-31-methoxycyclohexyl ring is situated in a shallow groove next to the main binding pocket. The pyrane ring and the macrocycle of FK506 appear to form a scaffold to position the methyl groups at C_{11}, C_{17} and C_{25} and the methoxy group at C_{15} for van der Waals contacts. The segment between atoms C_{18} and C_{23} of FK506 does not contact FKBP51 (Fig. 5c). In the crystal lattice these residues face a solvent channel and thus are rather poorly ordered.

Upon binding of FK506, the residues lining the rim of the hydrophobic pocket of FKBP51, Tyr57, Phe67, Asp68, Phe77 and Ile87, move sideways, widening the entrance to the binding site (Fig. 5c). The indole ring of residue Trp90 at the bottom of the binding pocket rotates slightly away from the pipecolate moiety of FK506. The conformational changes in FKBP51 are limited to the immediate vicinity of the ligand. The observed conformational changes around the ligand are quite similar to those of FKBP12 (and FKBP12.6), the primary physiological target of FK506, which is consistent with the absolute conservation of the respective residues between the two PPIases (Fig. 5d). In contrast to FKBP12, however, the tip of the loop connection between $\beta5$ and $\beta6$, residues 118 and 119, does not move towards the ligand in FKBP51. This might be caused by considerable sequence differences in this segment. In the FKBP12–FK506 complex, His87 (corresponding to position 118 in FKBP51) stacks upon the pyrane ring in FK506. The

lack of this hydrophobic contact might explain the lower affinity observed for FKBP51 compared with FKBP12 (Kozany *et al.*, 2009).

Interestingly, electron density for two well defined water molecules was observed in the space between the ligand and the loop of the FKBP51–FK506 structure, forming a chain of hydrogen bonds between Ser118, the backbone N atom of Lys121 and the 3-methoxy group in the cyclohexyl group of FK506. A similar conserved water molecule was also observed in most apo structures of FKBP51, indicating that a hydrogen-bond acceptor to satisfy the backbone amide of Lys121 might be important for the integrity of the Ser118–Lys121 loop.

In the apo structure of crystal form IV (PDB entry 3o5p), 14 water molecules were resolved in the binding pocket. Three of these occupied positions similar to the hydrogen acceptors in FK506 discussed above. Well defined active-site water molecules have also been identified in corresponding positions in crystal form VI (PDB entry 3o5e) and in a high-resolution structure of FKBP12 (PDB entry 2ppn; Szep *et al.*, 2009). In particular, the backbone amide of Ile87 was hydrogen bonded in all higher resolution structures (PDB entries 3o5e–3o5g and 3o5k–3o5r), indicating that satisfying the Ile87 amide might be particularly important. Interestingly, PEG and DMSO were bound to the Ile87 amide instead of water in two of the FKBP51 structures (PDB entries 3o5l and 3o5q), respectively. These findings presumably reflect the strong hydrophobicity of the binding pocket. Nevertheless, the displacement of 14 ordered water molecules from the binding pocket by FK506 should result in a considerable entropic contribution to the binding energy.

4. Outlook

FKBP51 ligands offer the potential to modulate steroid hormone responsiveness, which is particularly attractive in the light of its physiological role and its well documented association with psychiatric disorders. Given the antagonistic effects of FKBP51 and FKBP52, however, any useful pharmacological tool or lead compound is likely to have to discriminate between these two close homologues. A precise structural understanding of the FKBP51 binding site is extremely important for the rational design of such compounds. Based on the series of high-resolution structures presented in this report, the 71–74 bulge and the 118–122 loop emerge as the most promising parts of the binding pocket to achieve selectivity. Since these regions are highly flexible, interactions with potential ligands are likely to induce adaptive conformational rearrangements that are difficult to predict beforehand. Therefore, the determination of additional high-resolution complex structures will be crucial for an efficient design process. The crystallization conditions identified in this work should be excellently suited for this purpose.

References

Becker, J. W., Rotonda, J., McKeever, B. M., Chan, H. K., Marcy, A. I., Wiederrecht, G., Hermes, J. D. & Springer, J. P. (1993). *J. Biol. Chem.* **268**, 11335–11339.

Binder, E. B. (2009). *Psychoneuroendocrinology*, **34**, S186–S195.

Cheung-Flynn, J., Prapapanich, V., Cox, M. B., Riggs, D. L., Suarez-Quian, C. & Smith, D. F. (2005). *Mol. Endocrinol.* **19**, 1654–1666.

Deivanayagam, C. C. S., Carson, M., Thotakura, A., Narayana, S. V. L. & Chodavarapu, R. S. (2000). *Acta Cryst.* D**56**, 266–271.

DeLano, W. L. (2002). *PyMOL.* http://www.pymol.org.

Dornan, J., Taylor, P. & Walkinshaw, M. D. (2003). *Curr. Top. Med. Chem.* **3**, 1392–1409.

Dubowchik, G. M., Vrudhula, V. M., Dasgupta, B., Ditta, J., Chen, T., Sheriff, S., Sipman, K., Witmer, M., Tredup, J., Vyas, D. M., Verdoorn, T. A., Bollini, S. & Vinitsky, A. (2001). *Org. Lett.* **3**, 3987–3990.

Echeverria, P. C. & Picard, D. (2010). *Biochim. Biopys. Acta*, **1803**, 641–649.

Evans, P. R. (1997). *Jnt CCP4/ESF–EACBM Newsl. Protein Crystallogr.* **33**, 22–24.

French, S. & Wilson, K. (1978). *Acta Cryst.* A**34**, 517–525.

Galat, A. (2008). *J. Chem. Inf. Model.* **48**, 1118–1130.

Galigniana, M. D., Harrell, J. M., O'Hagen, H. M., Ljungman, M. & Pratt, W. B. (2004). *J. Biol. Chem.* **279**, 22483–22489.

Gouet, P., Courcelle, E., Stuart, D. I. & Métoz, F. (1999). *Bioinformatics*, **15**, 305–308.

Griffith, J. P., Kim, J. L., Kim, E. E., Sintchak, M. D., Thomson, J. A., Fitzgibbon, M. J., Fleming, M. A., Caron, P. R., Hsiao, K. & Navia, M. A. (1995). *Cell*, **82**, 507–522.

Holt, D. A., Luengo, J. I., Yamashita, D. S., Oh, H. J., Konilian, A. L., Yen, H. K., Rozamus, L. W., Brandt, M., Bossard, M. J., Levy, M. A., Eggleston, D. S., Liang, J., Schultz, W., Stout, T. J. & Clardy, J. (1993). *J. Am. Chem. Soc.* **115**, 9925–9938.

Horstmann, M., Ehses, P., Schweimer, K., Steinert, M., Kamphausen, T., Fischer, G., Hacker, J., Rösch, P. & Faber, C. (2006). *Biochemistry*, **45**, 12303–12311.

Itoh, S., DeCenzo, M. T., Livingston, D. J., Pearlman, D. A. & Navia, M. A. (1995). *Bioorg. Med. Chem. Lett.* **5**, 1983–1988.

Kabsch, W. (2010). *Acta Cryst.* D**66**, 125–132.

Kozany, C., März, A., Kress, C. & Hausch, F. (2009). *Chembiochem*, **10**, 1402–1410.

Laskowski, R. A., MacArthur, M. W., Moss, D. S. & Thornton, J. M. (1993). *J. Appl. Cryst.* **26**, 283–291.

Leslie, A. G. W. (1992). *Jnt CCP4/ESF–EACBM Newsl. Protein Crystallogr.* **26**.

Li, P., Ding, Y., Wu, B., Shu, C., Shen, B. & Rao, Z. (2003). *Acta Cryst.* D**59**, 16–22.

Liang, J., Hung, D. T., Schreiber, S. L. & Clardy, J. (1996). *J. Am. Chem. Soc.* **118**, 1231–1232.

Maestre-Martínez, M., Edlich, F., Jarczowski, F., Weiwad, M., Fischer, G. & Lücke, C. (2006). *J. Biomol. NMR*, **34**, 197–202.

Maestre-Martínez, M., Haupt, K., Edlich, F., Neumann, P., Parthier, C., Stubbs, M. T., Fischer, G. & Luecke, C. (2011). *J. Mol. Recognit.* **24**, 23–34.

Murshudov, G. N., Skubák, P., Lebedev, A. A., Pannu, N. S., Steiner, R. A., Nicholls, R. A., Winn, M. D., Long, F. & Vagin, A. A. (2011). *Acta Cryst.* D**67**, 355–367.

Ni, L., Yang, C.-S., Gioeli, D., Frierson, H., Toft, D. O. & Paschal, B. M. (2010). *Mol. Cell. Biol.* **30**, 1243–1253.

Paulini, R., Müller, K. & Diederich, F. (2005). *Angew. Chem. Int. Ed. Engl.* **44**, 1788–1805.

Pereira, P. J., Vega, M. C., González-Rey, E., Fernández-Carazo, R., Macedo-Ribeiro, S., Gomis-Rüth, F. X., González, A. & Coll, M. (2002). *EMBO Rep.* **3**, 88–94.

Periyasamy, S., Hinds, T., Shemshedini, L., Shou, W. & Sanchez, E. R. (2010). *Oncogene*, **29**, 1691–1701.

Perrakis, A., Morris, R. & Lamzin, V. S. (1999). *Nature Struct. Biol.* **6**, 458–463.

Potterton, E., Briggs, P., Turkenburg, M. & Dodson, E. (2003). *Acta Cryst.* D**59**, 1131–1137.

Pratt, W. B., Morishima, Y. & Osawa, Y. (2008). *J. Biol. Chem.* **283**, 22885–22889.

Riboldi-Tunnicliffe, A., König, B., Jessen, S., Weiss, M. S., Rahfeld, J., Hacker, J., Fischer, G. & Hilgenfeld, R. (2001). *Nature Struct. Biol.* **8**, 779–783.

Riggs, D. L., Cox, M. B., Tardif, H. L., Hessling, M., Buchner, J. & Smith, D. F. (2007). *Mol. Cell. Biol.* **27**, 8658–8669.

Rotonda, J., Burbaum, J. J., Chan, H. K., Marcy, A. I. & Becker, J. W. (1993). *J. Biol. Chem.* **268**, 7607–7609.

Saul, F. A., Arié, J. P., Vulliez-le Normand, B., Kahn, R., Betton, J. M. & Bentley, G. A. (2004). *J. Mol. Biol.* **335**, 595–608.

Schüttelkopf, A. W. & van Aalten, D. M. F. (2004). *Acta Cryst.* D**60**, 1355–1363.

Sheldrick, G. M. (2008). *Acta Cryst.* A**64**, 112–122.

Sinars, C. R., Cheung-Flynn, J., Rimerman, R. A., Scammell, J. G., Smith, D. F. & Clardy, J. (2003). *Proc. Natl Acad. Sci. USA*, **100**, 868–873.

Smith, D. F. & Toft, D. O. (2008). *Mol. Endocrinol.* **22**, 2229–2240.

Sun, F., Li, P., Ding, Y., Wang, L., Bartlam, M., Shu, C., Shen, B., Jiang, H., Li, S. & Rao, Z. (2003). *Biophys. J.* **85**, 3194–3201.

Szep, S., Park, S., Boder, E. T., Van Duyne, G. D. & Saven, J. G. (2009). *Proteins*, **74**, 603–611.

Theobald, D. L. & Wuttke, D. S. (2006a). *Bioinformatics*, **22**, 2171–2172.

Theobald, D. L. & Wuttke, D. S. (2006b). *Proc. Natl Acad. Sci. USA*, **103**, 18521–18527.

Theobald, D. L. & Wuttke, D. S. (2008). *PLoS Comput. Biol.* **4**, e43.

Tranguch, S., Cheung-Flynn, J., Daikoku, T., Prapapanich, V., Cox, M. B., Xie, H., Wang, H., Das, S. K., Smith, D. F. & Dey, S. K. (2005). *Proc. Natl Acad. Sci. USA*, **102**, 14326–14331.

Vagin, A. & Teplyakov, A. (2010). *Acta Cryst.* D**66**, 22–25.

Van Duyne, G. D., Standaert, R. F., Karplus, P. A., Schreiber, S. L. & Clardy, J. (1991). *Science*, **252**, 839–842.

Van Duyne, G. D., Standaert, R. F., Schreiber, S. L. & Clardy, J. (1991). *J. Am. Chem. Soc.* **113**, 7433–7434.

Weiwad, M., Edlich, F., Kilka, S., Erdmann, F., Jarczowski, F., Dorn, M., Moutty, M. C. & Fischer, G. (2006). *Biochemistry*, **45**, 15776–15784.

Westberry, J. M., Sadosky, P. W., Hubler, T. R., Gross, K. L. & Scammell, J. G. (2006). *J. Steroid Biochem. Mol. Biol.* **100**, 34–41.

Wilson, K. P., Yamashita, M. M., Sintchak, M. D., Rotstein, S. H., Murcko, M. A., Boger, J., Thomson, J. A., Fitzgibbon, M. J., Black, J. R. & Navia, M. A. (1995). *Acta Cryst.* D**51**, 511–521.

Winn, M. D. *et al.* (2011). *Acta Cryst.* D**67**, 235–242.

Wu, B., Li, P., Liu, Y., Lou, Z., Ding, Y., Shu, C., Ye, S., Bartlam, M., Shen, B. & Rao, Z. (2004). *Proc. Natl Acad. Sci. USA*, **101**, 8348–8353.

Yang, Z., Wolf, I. M., Chen, H., Periyasamy, S., Chen, Z., Yong, W., Shi, S., Zhao, W., Xu, J., Srivastava, A., Sánchez, E. R. & Shou, W. (2006). *Mol. Endocrinol.* **20**, 2682–2694.

Yong, W., Yang, Z., Periyasamy, S., Chen, H., Yucel, S., Li, W., Lin, L. Y., Wolf, I. M., Cohn, M. J., Baskin, L. S., Sánchez, E. R. & Shou, W. (2007). *J. Biol. Chem.* **282**, 5026–5036.